

6,6″-Azobis(2,2′-bipyridine) and Its Dinuclear Ruthenium Complex: A Comparative Study with Positional Isomers

Joe Otsuki,* Izumi Kurihara, Arata Imai, Yuki Hamada, and Nobuyuki Omokawa

College of Science and Technology, Nihon University, 1-8-14 Kanda Surugadai, Chiyoda-ku, Tokyo 101-8308

Received July 14, 2006; E-mail: otsuki@chem.cst.nihon-u.ac.jp

The azobis(bipyridine) ligand 6,6″-azobis(2,2′-bipyridine) (6-azobpy) was prepared as a new member of the family of azopolypyridine derivatives. This compound undergoes reversible trans/cis photoisomerization. Reaction of 6-azobpy and $[Ru(bpy)_2Cl_2]$ afforded a dinuclear complex $[\{Ru(bpy)_2\}_2(\mu\text{-}6\text{-azobpy})]^{4+}$. An analogue with deuterated bpy fragments was also prepared to help clarify the ^{1}H NMR signals in the part of the 6-azobpy ligand. The analysis of ^{1}H NMR spectra clearly identified the structure of the complex, in which the Ru^{2+} ions are chelated by the bpy parts of the bridging 6-azobpy ligand. Electronic absorption and electrochemical properties are characterized by the presence of a low-lying π^* level of the bridging ligand, manifested by a metal-to-ligand charge-transfer band extending down to 800 nm and by two consecutive one-electron reduction waves at relatively less negative potentials in cyclic voltammetry. These properties were compared with those of previously reported positional isomers with the help of density functional theory (DFT), time-dependent DFT, and ZINDO calculations. The analysis of the redox couple of $Ru^{3+/2+}$ showed that the redox potentials differ slightly between the diastereomers and that there is an intermetallic electronic interaction.

Ruthenium polypyridine complexes have attracted intense interest because of their favorable optical and electronic properties for light emission and electron/energy-transfer processes.[1] Multicentered oligo/polymetal complexes have thus been prepared to obtain insight into electronic communication among metal centers within the supramolecular framework. Understanding these oligo/polymetal complexes may lay the foundation for the materialization of molecular scale electronic/optical devices based on the rich redox/optical properties of metal complexes.

In multimetal complexes, the bridging ligand connecting metal complex units plays a pivotal role in determining the electronic communication between the metal complex units.[1] A large number of bridging ligands have been developed and tested from various points of views. Especially, π-conjugated bridges have attracted special attention, since the delocalized electronic structures in these bridges are advantageous for mediating electronic communication between the redox/photoactive metal complex units located at both ends. Furthermore, the structural rigidity of π-conjugated bridges affords well-defined geometry.

We have prepared and investigated a series of Ru and Os complexes containing 4,4″-azobis(2,2′-bipyridine) (4-azobpy),[2] 5,5″-azobis(2,2′-bipyridine) (5-azobpy),[3] or 4′,4‴″-azobis(2,2′:6′,2″-terpyridine) (4-azotpy)[4] (Chart 1). Some of these complexes, that is, complexes containing 4-azobpy or 4-azotpy, behave as molecular light switches responding to redox input, and a complex that contains 5-azobpy shows complex-sensitized photoisomerization. We prepared a new member of the family, i.e., 6,6″-azobis(2,2′-bipyridine) (6-azobpy) in the present study. The dinuclear complex Ru(6-azobpy)Ru is unique in the family because the metal–metal distance is the shortest and the surroundings of the $Ru(bpy)_3^{2+}$ core are more sterically congested. Thus, our expectation was that these characteristics may lead to novel properties.[5] Herein, we report the preparation and properties of the ligand and its dinuclear Ru complex, which are compared with those of 4- and 5-azobpy ligands and their Ru complexes.

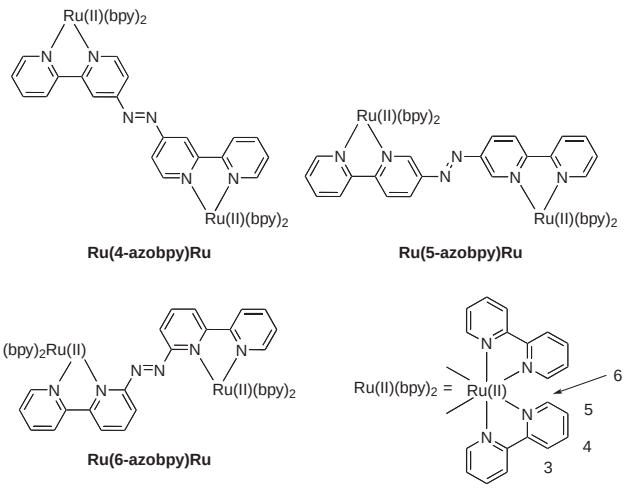

Chart 1.

Experimental

Instruments and Measurements. ^{1}H NMR spectra were recorded on a JEOL GX-400 spectrometer. Electron impact high-resolution mass spectroscopy (EI-HRMS) was performed by the Chemical Analysis Center of the School of Medicine, Nihon University. Electron impact mass spectra (EI-MS) were recorded on a Shimadzu QP5050A mass spectrometer. Electrospray ionization mass spectra (ESI-MS) were obtained with a JEOL JMS-600H mass spectrometer. Elemental Analyses were performed by the Chemical Analysis Center of the College of Science and Technology, Nihon University.

Published on the web May 14, 2007; doi:10.1246/bcsj.80.902

Absorption spectra were acquired with a Shimadzu UV-2400PC spectrometer in a 1 × 1 cm quartz optical cell maintained at 25 °C with a Peltier thermostat. In isomerization experiments, the light source of a Shimadzu RF-5300PC fluorimeter was used as an excitation light, with a slit width of 20 nm.

Cyclic voltammetry measurements were carried out with a Hokuto Denko HZ-3000 voltammetric analyzer. The electrochemical cell, maintained under N_2, was equipped with a Pt disk working electrode, a Pt wire counter electrode, and an Ag/Ag^+ (0.01 M $AgNO_3$ and 0.1 M Bu_4NPF_6 in CH_3CN) reference electrode. These electrodes were purchased from BAS. The supporting electrolyte solution was 0.1 M Bu_4NPF_6 in CH_3CN or CH_2Cl_2. The scan rate was 100 mV s^{-1} unless otherwise noted. Potentials are reported with respect to the internal ferrocenium/ferrocene (Fc^+/Fc) couple added after each measurement. Digital simulations of cyclic voltammograms were conducted using DigiSim, BAS.

Molecular Orbital Calculations. Density functional theory (DFT) calculations were performed using the Gaussian 03w program package on a personal computer.[6] We used the B3LYP functional[7] for all the calculations. The molecular orbital calculations for the uncomplexed ligands were carried out using the 6-31+G(d) basis set on the structures optimized by B3LYP/6-31G(d). Time-dependent DFT calculations were performed for the free ligands also using B3LYP/6-31+G(d). Electrical transitions expected to occur at >280 nm were calculated. For the complexes, Ru(4-azobpy)Ru and Ru(5-azobpy)Ru, B3LYP/LanL2DZ was employed for geometry optimization and molecular orbital calculations. The optimization was performed with a C_i symmetry constraint. For the structure optimization of Ru(6-azobpy)Ru ($\Lambda\Lambda$ and meso), the basis set LanL2DZ with an effective core approximation was used only for the Ru atoms, and the 3-21G set, which has a smaller number of primitive Gaussians, was used for the other atoms. This was to save the calculation time, since the symmetry constraint had to be lifted to find stable geometries for these complexes. The final molecular orbital calculations on the optimized structures were carried out using LanL2DZ for all atoms to obtain consistent results with other complexes. Electronic spectra for the dinuclear complexes were simulated by ZINDO[8] implemented in a CAChe program. The calculations were carried out with configuration interaction level 8 and INDO/1 parameters on the complexes optimized by DFT as described above.

Materials. The ligand, 6-azobpy, and its dinuclear Ru complex, Ru(6-azobpy)Ru, were prepared according to Scheme 1. Toluene was distilled over Na. Other solvents were used as received.

6-Nitro-2,2′-bipyridine. 2-Bromo-6-nitropyridine[9] (1.69 g, 8.32 mmol) and $[Pd(Ph_3P)_4]$ (0.96 g, 0.83 mmol) were put in a flask, the air was then replaced by Ar using a vacuum/Ar manifold, and toluene (110 mL) was added. A solution of 2-trimethylstannylpyridine[10] (2.04 g, 8.40 mmol) in toluene purged with Ar was added, and the mixture was refluxed for 16 h. After the reaction mixture was filtered to remove insoluble materials, the solvent was evaporated and the residue chromatographed (SiO_2, CH_2Cl_2) to afford a slightly yellowish solid (1.19 g, 5.91 mmol, 71%). ^{1}H NMR ($CDCl_3$): δ 7.40 (1H, ddd, J = 8 Hz, 4.8 Hz, 0.8 Hz, py-5′), 7.89 (1H, td, J = 8 Hz, 1.2 Hz, py-4′), 8.15 (1H, t, J = 8 Hz, py-4), 8.25 (1H, d, J = 8 Hz, py-5), 8.56 (1H, dd, J = 8 Hz, 0.8 Hz, py-3′), 8.71 (1H, dd, J = 4.8 Hz, 1.2 Hz, py-6′), 8.83 (1H, d, J = 8 Hz, py-3). EI-HRMS: calcd for $C_{10}H_7N_3O_2$: 201.0538; found: 201.0536.

6-Azobpy. Zn powder (3.0 g) was added portionwise to a solution of 6-nitro-2,2′-bipyridine (300 mg, 1.49 mmol) in THF (60 mL) (CAUTION!: Zn powder might catch fire). An aqueous NaOH solution (1 g/2.5 mL) was then added dropwise, and the mixture was stirred at room temperature for 6 h. The reaction mixture was filtered, and the solid was extracted with CH_2Cl_2. The combined solution was evaporated to give a purple solid. This was passed through an Al_2O_3 column with CH_2Cl_2 to remove the purple material to afford an orange solid, which was crystallized from benzene to give orange needles (170 mg, 0.50 mmol, 67%). ^{1}H NMR ($CDCl_3$): δ 7.37 (2H, ddd, J = 7.6 Hz, 4.8 Hz, 1.2 Hz, py-5′), 7.88 (2H, td, J = 7.6 Hz, 1.8 Hz, py-4′), 7.96 (2H, dd, J = 7.6 Hz, 0.8 Hz, py-5), 8.08 (2H, t, J = 7.6 Hz, py-4), 8.64 (2H, dd, J = 7.6 Hz, 0.8 Hz, py-3), 8.67 (2H, ddd, J = 7.6 Hz, 1.2 Hz, 0.8 Hz, py-3′), 8.73 (2H, ddd, J = 4.8 Hz, 1.2 Hz, 0.8 Hz, py-6′). EI-MS: m/z = 339 (M^+). Anal. Calcd for $C_{20}H_{14}N_6$: C, 70.99; H, 4.17; N, 24.84%. Found: C, 70.91; H, 4.41; N, 24.70%.

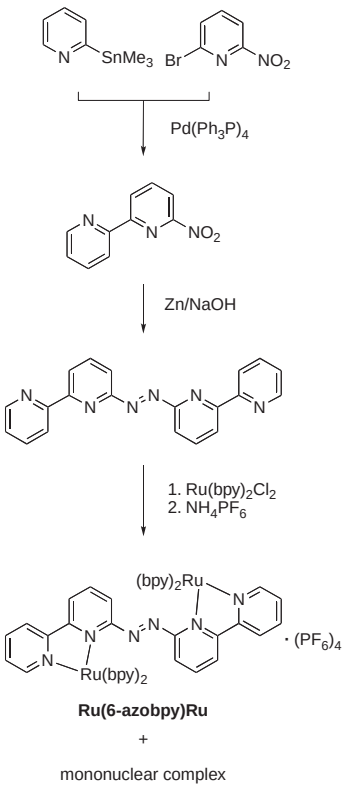

Scheme 1.

Ru(6-azobpy)Ru. A solution of 6-azobpy (110 mg, 1.28 mmol) and *cis*-$[Ru(bpy)_2Cl_2]\cdot 2(H_2O)$[11] (666 mg, 0.32 mmol) in EtOH (150 mL) was refluxed for 34 h under Ar. The solvent was evaporated, and H_2O was added to the residue. After removing the insoluble materials by filtration, NH_4PF_6 was added, and the mixture was stirred well. The precipitated black solid was chromatographed (SiO_2, CH_3CN/0.4 M aqueous KNO_3 (3/1)). NH_4PF_6 was added to the isolated fraction, and the solvent concentrated to remove CH_3CN and to precipitate out the PF_6^- salt of the desired complex as a dark green solid (156 mg, 0.09 mmol, 28%). A mononuclear complex, $[Ru(6\text{-azobpy})(bpy)_2]$, was also obtained, which has not been fully characterized. ^{1}H NMR ($CDCl_3$): see Results and Discussion section. ES-MS: m/z = 1600 ($[M-(PF_6)]^+$), 728 ($[M-2(PF_6)]^{2+}$). Anal. Calcd for $C_{60}H_{46}F_{24}N_{14}P_4Ru_2$: C, 41.30; H, 2.66; N, 11.24%. Found: C, 41.10; H, 2.91: N, 11.15%.

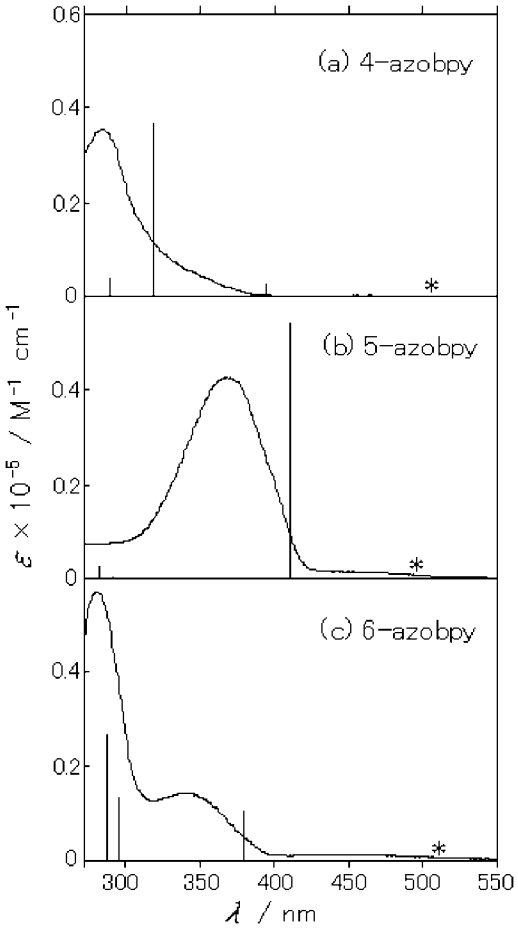

Fig. 1. Absorption spectra for azobpy's in DMF. Vertical bars are relative oscillator strengths according to time-dependent DFT calculations. Asterisks indicate the calculated positions of nπ^* transitions.

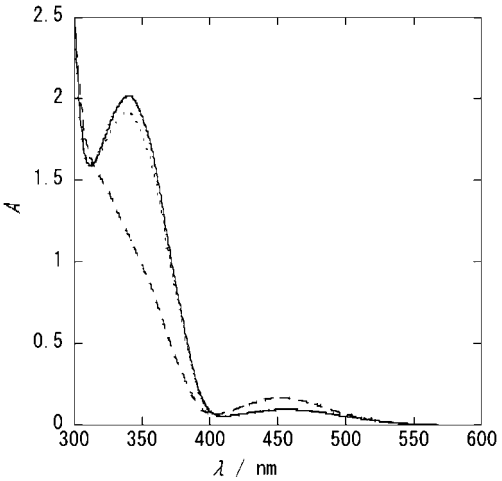

Fig. 2. Absorption spectra for 6-azobpy in the trans configuration (solid line) and in the photostationary states under 340 nm (dashed line) and 450 nm (dotted line) irradiation. The spectra were measured in DMF (0.1 mM).

Results and Discussion

Spectroscopic and Electronic Properties of the Ligands. The absorption spectra for 4-, 5-, and 6-azobpy are shown in Fig. 1. The spectra are distinctly different depending on the substitution positions of the azo group. For 4-azobpy, only one major peak appears at a short wavelength of 284 nm. For 5-azobpy, an intense peak appears at 369 in addition to a weak absorption around 450 nm. For 6-azobpy, there are two relatively intense peaks at 280 and 341 nm in addition to a weak absorption around 450 nm. Time-dependent DFT calculations were performed to shed light on the origin of these absorption bands. We used B3LYP/6-31+G(d) for the time-dependent DFT calculations on the structures optimized by B3LYP/6-31G(d). The obtained transition wavelengths are indicated by vertical bars, of which the height is proportional to the calculated oscillator strength, in Fig. 1. The numerical data for the transitions (Table S1) and pictorial illustration of HOMO and LUMO (Fig. S1) are given in Supporting Information.

Comparison of the three spectra in Fig. 1 reveals that the low intensity absorption around 450 nm appears for 5- and 6-azobpy's, but not for 4-azobpy. The calculations showed that there are nπ^* excited states at energy around 2.5 eV (≈500 nm), which are shown by asterisks on the graph. Thus, the low-intensity, low-energy absorption bands were assigned to the nπ^* band. Unfortunately, calculations on the idealized planar geometry gave a zero oscillator strength for the nπ^* transition and did not provide information as to why only 4-azobpy does not exhibit this absorption band.

On the other hand, for intense absorption bands at the shorter wavelength region (280–420 nm), the calculations predicted the spectral shape quite correctly, although the transition energies were a little underestimated. The lowest energy transition in this spectral range is the HOMO to LUMO $\pi\pi^*$ transition, which was predicted to be around 380–410 nm by the calculation and observed around 340–370 nm. The transitions of higher energies around 300 nm are other $\pi\pi^*$ transitions. The correctly reproduced results in the calculations are as follows. (i) 4-Azobpy exhibits a very weak HOMO to LUMO transition, while higher energy transitions are strong. (ii) 5-Azobpy exhibits a strong HOMO to LUMO transition, while higher energy transitions are weak. (iii) 6-Azobpy exhibits a spectrum with two peaks, in which the lower and higher energy peaks may correspond to the HOMO to LUMO transition and other $\pi\pi^*$ transitions, respectively.

Inspection of the molecular orbitals gave a hint for a very small oscillator strength for the HOMO to LUMO transition in 4-azobpy. As shown in Fig. S1, the LUMO of azobpy is concentrated on the azo and inner pyridine moieties, while the HOMO is on the bipyridines, but not on the azo moiety. Thus, these orbitals only overlap on the inner pyridines, which may account for the small oscillator strength. For 5-azobpy, both of the HOMO and LUMO are delocalized over the entire molecule. For 6-azobpy, the HOMO and LUMO are overlapped each other on the inner pyridine and the azo moieties.

Upon excitation into the $\pi\pi^*$ absorption band of *trans*-6-azobpy, the $\pi\pi^*$ band decreased, and the nπ^* band increased, with isosbestic points at 314 and 405 nm, until reaching a photostationary state, as shown in Fig. 2. This is a typical trans-to-cis photoisomerization for azobenzene and azopyridine derivatives.[12,13] The $\pi\pi^*$ peak decreased to become a mere shoulder of a shorter absorption band, implying the cis content under

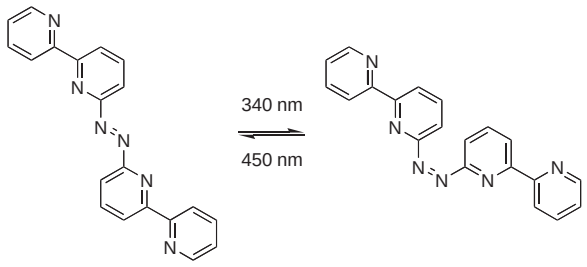

Scheme 2.

these conditions is large. Upon subsequent irradiation of the $n\pi^*$ band at 450 nm, the absorption spectrum nearly changed back to the original spectrum, which corresponds to the cis-to-trans conversion, as shown in Scheme 2. Thus, 6-azobpy as well as 5-azobpy[3] underwent reversible photoisomerization, while 4-azobpy did not show any spectral change upon light irradiation.

Cyclic voltammogram for 6-azobpy in CH_2Cl_2 had a reduction peak at a potential similar to those of 4-[2] and 5-azobpy[3] ligands. The wave at -1.38 V vs Fc^+/Fc corresponds to the first one-electron reduction. The second one-electron reduction,[14,15] expected around -1.8 V may be located slightly out of the potential window (≤ -2.0 V). The first reduction was reversible in the sense that the ratio of cathodic to anodic current was near unity. However, the electron-transfer reaction seemed slower than the diffusion-limited rate, since the peak separation is large: 300–370 mV at scan rates of 50–200 mV s^{-1}.

Structure of Ru(6-azobpy)Ru. The ligand 6-azobpy was reacted with the $[Ru(bpy)_2Cl_2]$ fragment according to a standard procedure. This reaction afforded mononuclear and dinuclear complexes, from which the latter was isolated with column chromatography. The composition of the dinuclear complex $[\{Ru(bpy)_2\}_2(\mu\text{-6-azobpy})]$ was confirmed unambiguously by ESI-MS and elemental analysis. However, the ^{1}H NMR spectrum, as shown in the top of Fig. 3a, is quite complicated even with the help of two-dimensional ^{1}H NMR techniques. A part of the difficulty comes from the fact that the pattern of ^{1}H NMR spectrum for Ru(6-azobpy)Ru is quite different from those for other dinuclear complexes, since the bridging ligand and the auxiliary ligands are mutually closer due to geometrical reasons. Furthermore, caution must be taken in the structural characterization of a complex containing the 6-azobpy ligand, because it is, in principle, possible that a metal ion is chelated by nitrogen atoms from the pyridine ring and from the azo group.

Therefore, we prepared its analogue having deuterated bipyridine ligands by reacting 6-azobpy and $[Ru(bpy\text{-}d_8)_2Cl_2]$ to simplify the ^{1}H NMR spectra. The ^{1}H NMR spectrum thus obtained is shown in the lower part of Fig. 3a. In this spectrum, only protons on the 6-azobpy ligand are observed. To see whether these chemical shift values are reasonable for the structure shown in Chart 1, in which the two Ru^{2+} ions are chelated by the two bpy fragments, the chemical shifts of the complex in CD_3CN were compared to those of the ligand in $CDCl_3$, as shown in the lower part of Fig. 3b. Also shown in the figure (the top of Fig. 3b) are the chemical shifts of bpy in $CDCl_3$ and those of $[Ru(bpy)_3]^{2+}$ in CD_3CN. Upon the formation of the Ru complex, the chemical shifts for H-3, H-4, and

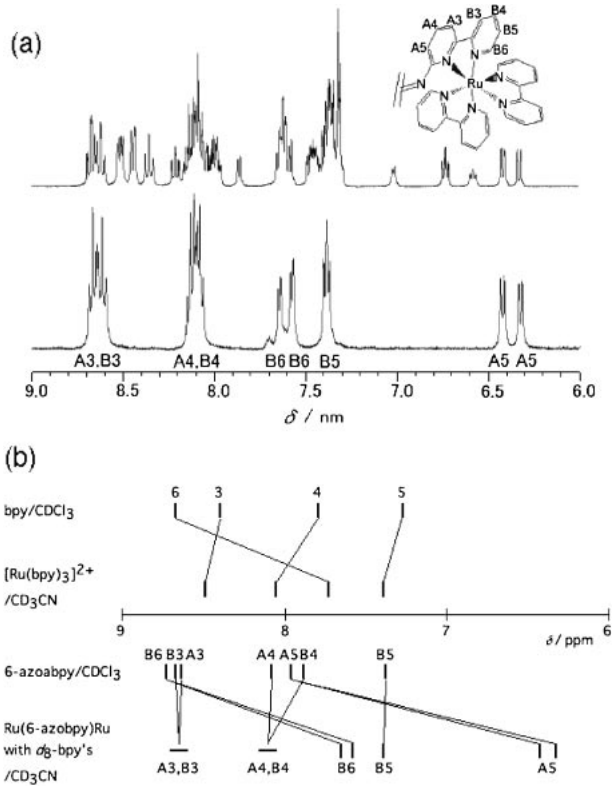

Fig. 3. ^{1}H NMR spectra for Ru(6-azobpy)Ru. (a) Ru(6-azobpy)Ru (top) and Ru(6-azobpy)Ru with deuterated bipyridines (bottom) in CD_3CN. (b) Comparison of chemical shifts of ligands in $CDCl_3$ and complexes in CD_3CN.

H-5 undergo moderate downfield shifts, while that for H-6 exhibits an upfield shift as large as 1.0 ppm (see Chart 1 for proton numbering). The latter upfield shift may be attributed to a ring current effect by the pyridine ring in the nearest bpy ligand. As for the 6-azobpy ligand in the dinuclear complex, chemical shift changes of protons on the B ring, which is the outer pyridine ring, were as expected from the results just mentioned for the model complex. This indicates that the chemical environment of the B ring is close to that of $[Ru(bpy)_3]^{2+}$ complex, consistent with a tris(bpy) type coordination. Especially, the large upfield shift of H-B6 by 1.1 ppm gives solid support for this type of coordination. The chemical shift changes of protons on the A ring were similar, except for H-A5. An upfield shift as large as 1.6 ppm was observed for H-A5. The DFT optimized molecular model of the Ru(6-azobpy)Ru indicated that this proton comes just on top of one of the auxiliary bpy ligand, which is expected to exert a large ring current effect, as shown in Fig. 4. In the figure, protons with a particularly large upfield shift and pyridine rings that cause the shift are related by arrows. It is apparent from the model that each of H-B6 and H-A5 lies on top of a pyridine ring. In particular, H-A5 protons are in a van der Waals contact with the face of the pyridine ring. Thus, this structure is fully consistent with the ^{1}H NMR data. Finally, it is noted that ^{1}H NMR resonances for the 6-azobpy ligand in Ru(6-azobpy)Ru are duplicated, which is clearly seen particularly for H-B6 and H-A5. This can be attributed to the diastereomers consisting of meso ($\Delta\Lambda$) and racemic ($\Delta\Delta$ and $\Lambda\Lambda$) compounds. The integration

values indicate that the as-prepared sample contained the isomers in a ratio of 6:4.

Spectroscopic and Electronic Properties of the Ru Dinuclear Complexes. The electronic absorption spectra for the series of Ru(azobpy)Ru are shown in Fig. 5a, and the numerical data are summarized in Table 1. Bands around 450 nm were common for all of the complexes. From the analogy to the parent complex $[Ru(bpy)_3]^{2+}$,[1] they may be assigned as the metal-to-ligand charge transfer (MLCT) bands, in which charge transfer, d(Ru) $\rightarrow \pi^*$(bpy), occurs on excitation. The most distinctive features in this class of complexes were the additional MLCT bands located to the lower energy side, which extend down to 800 nm. These may also be assigned as MLCT transitions, which are represented as d(Ru) $\rightarrow \pi^*$(azobpy). These assignments are supported by theoretical calculations as described below.

The structure optimization and molecular orbital calculations were carried out by DFT calculations. The pictorial representations for the HOMO and LUMO orbitals obtained by B3LYP/LanL2D2 are presented in Fig. S2. For all of these complexes, the HOMO was comprised of Ru dπ orbitals, while the LUMO lies on the azobpy bridging ligand. Absorption spectra were simulated by using the ZINDO method. We chose ZINDO, because it has been previously shown that it gives reliable results for Ru imine complexes.[16,17] The results of spectral simulation are shown in Fig. 5b. In the graph, an arbitrarily chosen linewidth of 3200 cm^{-1} was allotted to each transition. As can be seen from the simulated spectra, the spectral shape was reproduced quite well, although the transition energies were overestimated by ca. 7000 cm^{-1}. In the simulated spectra, the transitions above (lower in energy) and below (higher in energy) 360 nm corresponded to MLCT: d(Ru) $\rightarrow \pi^*$(azobpy) and MLCT: d(Ru) $\rightarrow \pi^*$(bpy), respectively. Intense transitions for the lower energy MLCT are characteristic

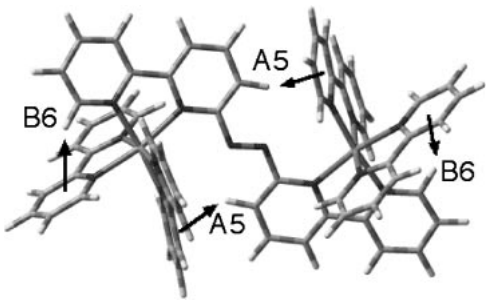

Fig. 4. DFT optimized structure of *meso*-Ru(6-azobpy)Ru. The protons on 6-azobpy that undergo a significant upfield shift and the pyridine rings that cause the shift by the ring current effect are related by the arrows.

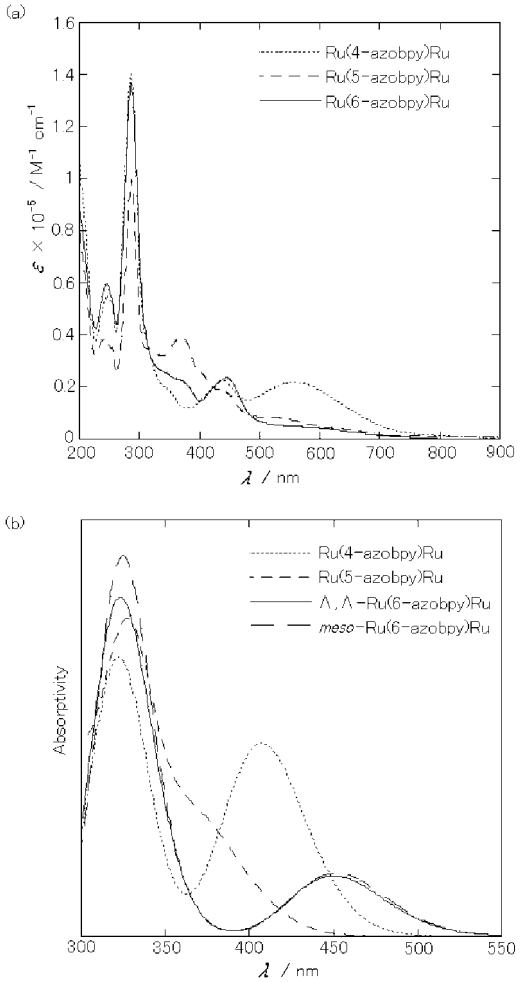

Fig. 5. Absorption spectra for dinuclear azobpy complexes. (a) Experimental spectra measured in CH_3CN. Dotted line: Ru(4-azobpy)Ru; dashed line: Ru(5-azobpy)Ru; solid line: Ru(6-azobpy)Ru. (b) Absorptivity as calculated by ZINDO. The linewidth of transitions were arbitrarily set at 3200 cm^{-1}. Dotted line: Ru(4-azobpy)Ru; dashed line: Ru(5-azobpy)Ru; solid line: ΛΛ-Ru(6-azobpy)Ru; *meso*-Ru(6-azobpy)Ru: long dashed line.

Table 1. Absorption and Redox Potentials of Dinuclear Complexes Bridged by Azobpy Ligands[a)]

	λ_{max}/nm ($\varepsilon \times 10^{-3}$/$cm^{-1}$ M^{-1})				$E^{\circ\prime}$/V vs Fc^+/Fc			
	MLCT	LC[b)]	MLCT (bpy)	MLCT (azo)	$bpy^{0/-1}$	$azo^{-1/-2}$	$azo^{0/-1}$	$Ru^{3+/2+}$ (ΔE_p/mV)[c)]
Ru(4-azobpy)Ru[d)]	245 (55)	286 (140)	439 (22)	558 (22)	≈ −1.8	−1.45	−0.92	0.95(82, 83)
Ru(5-azobpy)Ru[e)]	244 (39)	286 (99) 371 (39)	440 (19)	520 (9)	≈ −1.8	−1.15	−0.77	0.96(90, 81)
Ru(6-azobpy)Ru	242 (60)	286 (137) 365 (23)	449 (23)	~504 (5)	≈ −2.0	−1.29	−0.68	1.06(127, 70)
$[Ru(bpy)_3]^{2+}$	244 (29)	286 (86)	450 (14)		−1.73			1.01

a) In CH_3CN. b) Ligand centered. c) The first and second figures in parentheses are peak separations between the anodic and cathodic peaks for the $Ru^{3+/2+}$ couple and the internal Fc^+/Fc couple, respectively. d) Ref. 2. e) Ref. 3.

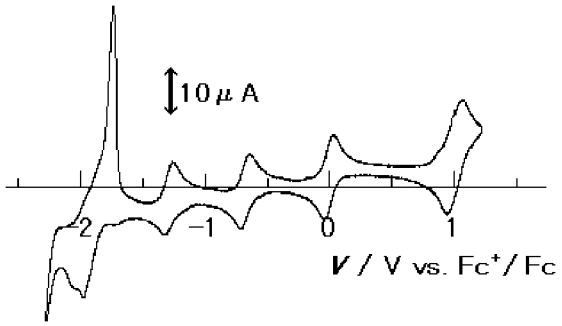

Fig. 6. Cyclic voltammogram for Ru(6-azobpy)Ru with internal ferrocene in CH_3CN.

to Ru(4-azobpy)Ru both in experiment and in theory. For Ru(5-azobpy)Ru and Ru(6-azobpy)Ru (both $\Lambda\Lambda$ and meso), the oscillator strengths for the lower energy transition were smaller, reproducing correctly the trend observed experimentally. All complexes exhibited transitions for the higher energy MLCT, i.e., d(Ru) $\rightarrow \pi^*$(bpy), in similar manners in terms of energy (observed at ca. 450 nm; calculated at ca. 320 nm) and intensity.

These dinuclear complexes, including Ru(6-azobpy)Ru, are hardly luminescent. Reduction of the 6-azobpy ligand did not lead to enhanced luminescence. Previously reported Ru(5-azobpy)Ru also does not show any redox responsive luminescence behavior.[3] The behavior is in contrast to that of Ru(4-azobpy)Ru, which shows a large luminescence enhancement upon reduction of the bridging ligand.[2]

Redox Properties of Ru(6-azobpy)Ru. Figure 6 shows the cyclic voltammogram for Ru(6-azobpy)Ru. The complex has redox centers at the metal ions, 6-azobpy, and bpy. On the cathodic scan, two waves corresponding to consecutive one-electron reductions of the bridging ligand appeared at -0.68 and -1.29 V, giving Ru(6-azobpy$^{\bullet-}$)Ru and Ru(6-azobpy^{2-})Ru, respectively. These reduced 6,6″-azobpy species in the complex are more stable when compared to the isolated ligand by 0.7 eV by the presence of positive charges of the pair of Ru^{2+} ions. The waves not only appeared at less negative potentials, but the reversibility of the waves improved as compared to the isolated ligand. Especially, the first reduction wave was completely reversible as far as the peak separation indicates under scan rates up to 200 mV s^{-1}. Waves for the reduction of the terminal bpy ligands were obscured by a spike peak probably due to adsorption/desorption of multiply reduced species to the electrode.

The Ru^{2+}/Ru^{3+} redox couple for Ru(6-azobpy)Ru appeared at 1.06 V. The peak separation of the anodic and cathodic peaks (ΔE_p) in this couple was 130 mV at a scan rate of 100 mV s^{-1}, distinctly larger than those of other complexes as shown in Table 1. This is also much larger than the value of $\approx$60 mV expected for a reversible electrode reaction for multiple noninteracting equivalent redox centers.[18] This can be, in principle, due to a slow electrode reaction and/or overlapping redox couples at slightly differing potentials. The peak separation was invariant at 127 ± 3 mV under scan rates in the range of 10–100 mV s^{-1}. This result indicated that the redox reaction is fast to the extent that the electrode reaction is diffusion limited. It leaves only the possibility that the redox wave contains more than one reversible couples overlapped with slightly shifted potentials.

Let us summarize relevant reactions before discussing more about the large peak separation. The electrode reactions are represented as:

$$Ru^{II}Ru^{II} \rightleftharpoons Ru^{II}Ru^{III} + e^-, \quad (1)$$

$$Ru^{II}Ru^{III} \rightleftharpoons Ru^{III}Ru^{III} + e^-, \quad (2)$$

wherein a simplified notation is used, e.g., $Ru^{II}Ru^{II}$ stands for Ru^{II}(6-azobpy)Ru^{II}. In addition, there is a conproportionation equilibrium in solution:

$$Ru^{II}Ru^{II} + Ru^{III}Ru^{III} \rightleftharpoons 2Ru^{II}Ru^{III}, \quad (3)$$

$$K_c = \frac{[Ru^{II}Ru^{III}]^2}{[Ru^{II}Ru^{II}][Ru^{III}Ru^{III}]} \quad (4)$$

where K_c is the conproportionation constant. The conproportionation constant is related to the redox potentials for the reactions 1 (E_1) and 2 (E_2) by:

$$K_c = \exp\left[\frac{F}{RT}(E_2 - E_1)\right], \quad (5)$$

where F, R, and T are the Faraday constant, the gas constant, and the absolute temperature, respectively. The conproportionation constant and the difference in the redox potentials are measures of the electronic interaction between the redox centers.

There are two possible reasons for the redox couple to split. One is that the splitting is due to electronic interactions between the two metallic centers. In this case, the equilibrium is shifted to the right-hand side in Eq. 3, giving rise to K_c larger than the noninteracting statistical value of 4. It was found by digital simulation that the difference between E_1 and E_2 was 77 mV, which corresponds to $K_c = 21$, accounting for the 127 mV peak separation. The other possibility is that the redox potentials between the meso and racemic diastereomers are different. This situation corresponds to the presence of two sets of equilibria represented by Eqs. 1–5, with E_1^{meso} and E_2^{meso} values being different from $E_1^{racemic}$ and $E_2^{racemic}$ values, respectively.

We found that the content of each isomer varies crop by crop in recrystallization. Needlelike crystals were obtained by diffusing CH_2Cl_2 vapor into a CH_3CN solution of Ru(6-azobpy)Ru, which contains both meso and racemic diastereomers. In our two different runs, we obtained samples consisting of isomers in ratios of 72:28 and 46:54, which are labeled A and B, respectively. These samples were subjected to cyclic voltammetry to investigate the effect of the composition change on the redox waves. If the large peak separation is exclusively due to an intermetallic interaction, the composition change should have no effect on the redox waves. If, on the other hand, the redox potentials are different between the diastereomers, the composition change should affect the redox waves. On going from sample A to sample B, the midpoint of the anodic and cathodic peaks in the Ru^{2+}/Ru^{3+} redox wave showed a small but measurable positive shift of 6 mV. That the composition change leads to shifts in redox peaks indicates that the redox potentials in the meso and racemic diastereomers are indeed different.

The problem now is whether the different redox potentials can be the sole reason for the large peak separation. To address this issue, digital simulations were carried out according to two sets of Eqs. 1–5 to see how peak positions change depending on the isomeric composition, assuming that there is no intermetallic electronic interaction ($K_c^{meso} = K_c^{racemic} = 4$). In the simulation, the difference in the redox potentials between the diastereomers was set as $E_1^{meso} - E_1^{racemic} = E_2^{meso} - E_2^{racemic} = \pm 77$ mV to best account for the peak separation. On going from the isomeric ratio of 72:28 to 46:54, the shape of the redox waves changed, and the midpoint of the anodic and cathodic peaks shifted by 22 mV. From the magnitude of the observed shifts, which were less than a third of what would be expected for the limiting case simulated above, it was concluded that the different redox potentials in the meso and racemic diastereomers can only explain a minor portion of the large peak separation. The remaining major part of the large peak separation then must be ascribed to an intermetallic electronic interaction. It is difficult to evaluate the conproportionation constant exactly, but it can be assumed that the value is somewhat smaller than the upper limit value of 21.[19]

The reason for the detection of an intermetallic interaction only for Ru(6-azobpy)Ru in the series listed in Table 1 may be that the metal–metal distance (r_{MM}) in Ru(6-azobpy)Ru is the shortest among them. The observed (X-ray) or estimated (DFT) r_{MM} values are as follows: 13.4 Å for Ru(4-azobpy)Ru (DFT), 10.0–11.8 Å for Ru(5-azobpy)Ru, depending on the conformation (X-ray[3]), and 8.2 Å for Ru(6-azobpy)Ru (DFT). Relevant values for related metal complexes were searched in the literature for comparison purposes. There are only a few reports on the metal–metal interactions across bpy–spacer–bpy type bridging ligands. Regarding the peak separation, $\Delta E_p = 100$, 90, and 90 mV have been reported for dinuclear Ru 2,2′-bipyridine complexes connected through a carbon–carbon triple bond at 4-, 5-, and 6-positions, respectively.[20] For another analogue, in which the spacer is an ethylenic double bond, $\Delta E_p = 90$ mV and $K_c = 15$ have been reported.[21]

Conclusion

We have prepared a bis-chelating ligand, 6-azobpy, as a new member of the azobpy family. In this family of 4-, 5-, and 6-azobpy's, the latter two ligands were found to be photochromic. The dinuclear Ru complex $[Ru_2(bpy)_4(6\text{-azobpy})]^{4+}$ was prepared. The ^{1}H NMR signals derived from the 6-azobpy part were extracted by using deuterated bpy auxiliary ligands. The simplified spectrum proved the structure of the complex as the tris(bipyridine) type dinuclear complex bridged by the 6-azobpy ligand. Absorption and electrochemical properties were compared with those of previously reported positional isomers, with the help of theoretical calculations. From the analysis of $Ru^{2+/3+}$ redox couple in cyclic voltammetry for Ru(6-azobpy)Ru, it was found that the meso and racemic compounds exhibit slightly different redox potentials. In addition, a metal–metal electronic interaction was detected with the conproportionation constant estimated to be a little less than 21. A shorter metal–metal separation in Ru(6-azobpy)Ru than those in the other positional isomers may be responsible for the intermetallic electronic interaction.

We thank I. Yoshikawa and Dr. T. Akasaka of the University of Tokyo for the ESI-MS measurements and help in spectroelectrochemistry, respectively. This work was partially supported by the "High-Tech Research Center" Project for Private Universities: matching fund subsidy from the Ministry of Education, Culture, Sports, Science and Technology, Japan.

Supporting Information

Absorption data and pictorial representation of molecular orbitals in PDF format. This material is available free of charge on the Web at: http://www.csj.jp/journals/bcsj/.

References

1 For reviews on Ru polypyridine complexes, see: a) A. Juris, V. Balzani, F. Barigelletti, S. Campagna, P. Belser, A. von Zelewsky, *Coord. Chem. Rev.* **1988**, *84*, 85. b) K. Kalyanasundaram, *Photochemistry of Polypyridine and Porphyrin Complexes*, Academic, London, **1992**. c) L. De Cola, P. Belser, *Coord. Chem. Rev.* **1998**, *177*, 301. d) C. Kaes, A. Katz, M. W. Hosseini, *Chem. Rev.* **2000**, *100*, 3553. e) F. Barigelletti, L. Flamigni, *Chem. Soc. Rev.* **2000**, *29*, 1. f) H. Hofmeier, U. S. Schubert, *Chem. Soc. Rev.* **2004**, *33*, 373.

2 a) J. Otsuki, D.-M. Li, K. Sato, A. Nakagome, T. Takido, I. Yoshikawa, T. Akasaka, K. Araki, *Bull. Chem. Soc. Jpn.* **2003**, *76*, 1185. b) J. Otsuki, M. Tsujino, T. Iizaki, K. Araki, M. Seno, K. Takatera, T. Watanabe, *J. Am. Chem. Soc.* **1997**, *119*, 7895. c) J. Otsuki, K. Sato, M. Tsujino, N. Okuda, K. Araki, M. Seno, *Chem. Lett.* **1996**, 847.

3 J. Otsuki, N. Omokawa, K. Yoshiba, I. Yoshikawa, T. Akasaka, T. Suenobu, T. Takido, K. Araki, S. Fukuzumi, *Inorg. Chem.* **2003**, *42*, 3057.

4 a) T. Akasaka, J. Otsuki, K. Araki, *Chem. Eur. J.* **2002**, *8*, 130. b) T. Akasaka, T. Mutai, J. Otsuki, K. Araki, *Dalton Trans.* **2003**, 1537.

5 Another aspect of our recent interest concerning oligo/polymetallic complexes is their ability to bind DNA double helices. We needed a set of dinuclear complexes systematically varied in structure. Studies on interactions between the complexes in Chart 1 and DNA double helices are in progress. See the following references: a) C. Metcalfe, J. A. Thomas, *Chem. Soc. Rev.* **2003**, *32*, 215. b) J. A. Smith, J. G. Collins, B. T. Patterson, F. R. Keene, *Dalton Trans.* **2004**, 1277. c) C. Rajput, R. Rutkaite, L. Swanson, I. Haq, J. A. Thomas, *Chem. Eur. J.* **2006**, *12*, 4611.

6 M. J. Frisch, G. W. Trucks, H. B. Schlegel, G. E. Scuseria, M. A. Robb, J. R. Cheeseman, J. A. Montgomery, Jr., T. Vreven, K. N. Kudin, J. C. Burant, J. M. Millam, S. S. Iyengar, J. Tomasi, V. Barone, B. Mennucci, M. Cossi, G. Scalmani, N. Rega, G. A. Petersson, H. Nakatsuji, M. Hada, M. Ehara, K. Toyota, R. Fukuda, J. Hasegawa, M. Ishida, T. Nakajima, Y. Honda, O. Kitao, H. Nakai, M. Klene, X. Li, J. E. Knox, H. P. Hratchian, J. B. Cross, V. Bakken, C. Adamo, J. Jaramillo, R. Gomperts, R. E. Stratmann, O. Yazyev, A. J. Austin, R. Cammi, C. Pomelli, J. W. Ochterski, P. Y. Ayala, K. Morokuma, G. A. Voth, P. Salvador, J. J. Dannenberg, V. G. Zakrzewski, S. Dapprich, A. D. Daniels, M. C. Strain, O. Farkas, D. K. Malick, A. D. Rabuck, K. Raghavachari, J. B. Foresman, J. V. Ortiz, Q. Cui, A. G. Baboul, S. Clifford, J. Cioslowski, B. B. Stefanov, G. Liu, A. Liashenko, P. Piskorz, I. Komaromi, R. L. Martin, D. J. Fox, T. Keith, M. A. Al-Laham, C. Y. Peng, A. Nanayakkara, M. Challacombe, P. M. W. Gill, B. Johnson, W. Chen, M. W. Wong, C. Gonzalez, J. A. Pople, *Gaussian 03, Revision C.02*, Gaussian, Inc., Walling-

ford CT, **2004**.
7 A. D. Becke, *J. Chem. Phys.* **1993**, *98*, 5648.
8 M. C. Zerner, *ZINDO Program, Quantum Theory Project*, University of Florida, Gainsesville, FL, U.S.A., **1998**.
9 J. W. Streef, H. J. den Hertog, *Recueil* **1969**, *88*, 1391.
10 G. V. Long, S. E. Boyd, M. M. Harding, I. E. Buys, T. W. Hambley, *J. Chem. Soc., Dalton Trans.* **1993**, 3175.
11 B. P. Sullivan, D. J. Salmon, T. J. Meyer, *Inorg. Chem.* **1978**, *17*, 3334.
12 E. V. Brown, G. R. Granneman, *J. Am. Chem. Soc.* **1975**, *97*, 621.
13 H. Rau, *Studies in Organic Chemistry 40: Photochromism, Molecules and Systems*, ed. by H. Dürr, H. Bouas-Laurent, Elsevier, Amsterdam, **1990**, p. 165.
14 A. J. Bellamy, I. S. MacKirdy, C. E. Niven, *J. Chem. Soc., Perkin Trans. 2* **1983**, 183.
15 J. L. Sadler, A. J. Bard, *J. Am. Chem. Soc.* **1968**, *90*, 1979.
16 S. I. Gorelsky, E. S. Dodsworth, A. B. P. Lever, A. A. Vlcek, *Coord. Chem. Rev.* **1998**, *174*, 469.
17 M. F. Ryan, R. A. Metcalfe, A. B. P. Lever, M. Haga, *J. Chem. Soc., Dalton Trans.* **2000**, 2357.
18 J. B. Flanagan, S. Margel, A. J. Bard, F. C. Anson, *J. Am. Chem. Soc.* **1978**, *100*, 4248.
19 An attempt to resolve the stepwise redox reactions with differential pulse voltammetry was unsuccessful. Also, we were unable to observe spectral changes upon partial oxidation of the Ru centers that could be attributed to the intervalence charge-transfer transition, possibly due to the overlapping absorption tail of the low-energy d(Ru) $\rightarrow \pi^*$(6-azobpy) MLCT band.
20 V. Grosshenny, A. Harriman, F. M. Romero, R. Ziessel, *J. Phys. Chem.* **1996**, *100*, 17472.
21 G. F. Strouse, J. R. Schoonover, R. Duesing, S. Boyde, W. E. Jones, Jr., T. J. Meyer, *Inorg. Chem.* **1995**, *34*, 473.